DOI: 10.13009/EUCASS2017-480

Effects of Wing Flexibility on the Drag of Regional Aviation Aircraft

Luis E. S. Garcia, Ana C. Meinicke, Júlio C. M. Rodrigues, Milton Santos and Adson A. de Paula
Instituto Tecnológico de Aeronáutica (ITA) - Department of Aircraft Design
São José dos Campos, SP, 12228-900, Brazil

Abstract

The influence of wing flexibility on aerodynamics is becoming of increasing importance given the current energy efficiency improvement of aircraft. The effects of wing bending and torsional flexibility on drag are analysed on a regional aviation aircraft wing-fuselage configuration for four different flight conditions using the BLWF software, a full-potential solver with an integral boundary layer subroutine. Several rigidity curves are modelled through Bezier curves and analysed. Drag comparisons between rigid and flexible wings are carried out, as well as variations of bending and torsional rigidities. As a result, it was observed that flexible wings tend to present higher drag values, due to an increase in induced and wave drag. It is mainly caused by the wing loading shifting from its outer to its inner part and also by the flow characteristic over a deformed wing. Therefore, an optimization design process should consider the flexible behaviour of the wing at the design point during the design phase for, i.e., determine the induced and wave drag after the accommodation of the wing to the flow over it on each design point.

1. Introduction

The global aviation industry has been facing significant economic and environmental challenges. Despite the increase in the value created to the users be evident, the aviation industry still presents one of the lowest profitability among all industries [1]. Moreover, on the environmental side, public awareness of this industry poluents emissions and aircraft noise led to strong pressure on the aviation business in order to find smarter and eco-friendly solutions [2]. In order to satisfy these stringent requirements new aeronautical technologies are being studied along the last decades, such as hybrid laminar flow control (HLFC), morphing devices, composite materials, sustainable fuels, electric taxiing systems, and many others. Besides the development of these new technologies, a simple way to increase the aircraft aerodynamic efficiency lies on the adoption of high aspect ratio (AR) wings. Boeing 747-400, for instance, has an aspect ratio of 8, which is 20% smaller than Boeing 777-300 (AR=10) and even smaller than Boeing 787 (AR=11). Another example is Embraer ERJ170 which has an aspect ratio of 8.6 which is quite small if compared to the Embraer E175-E2 (AR=12). Thereby, confirming this aerodynamic design trend.
However, the increase of the aspect ratio preserving the same wing area leads to a decrease in the chord length along the wing spanwise direction. This fact might yield to aeroelastic and aerodynamic undesired effects once the chord length is directly connected to the wing main box, which plays an important role in the wing rigidity.
The present work evaluates the impacts of the wing rigidity in the total drag for a regional aviation aircraft. Although flexibility effects on lift distribution seems to be known [3,4,5], here it is proposed to quantify these effects for the reference wing. In this investigation, several different rigidity profiles were considered in which some represented wings that are more flexible and others, more rigid. In addition, it was considered different regions on the spanwise to be introduced these variations. However, no structural stability nor aeroelastic criteria are studied. In this way, it would be possible to start defining integrated requirements, aerodynamic-structural, in order to determine how more flexible, or in other words more lighter, a wing can be, and in what regions of the spanwise, this reduction should be applied without jeopardizing performance. Moreover, this study could also be the starting point for a metamodel for conceptual studies and optimization of regional aircraft in which the flexibility effects could be evaluated in the early phases of a designing process.

DOI: 10.13009/EUCASS2017-480

2. Methodology

The analysis were conducted adopting as object of study a reference wing-body configuration from a regional airplane (low wing design, two-podded turbofan engines mounted below the wing) which main characteristics are presented on Table 1.

Table 1: Reference Wing main characteristics

Reference Wing Area [m2]	**Reference Chord [m]**	**Reference Span [m]**	**Number of Span Stations from the root to the wing tip**	**Number of Fuselage Stations**	**Fuselage Length [m]**
92.57	3.6835	27.77	15	58	37.7

The flexibility assessment was conducted taking into account the rigidity of the reference wing as presented on Fig. 1. These values were obtained by the calibration of the stiffness predicted through computational models with the ones measured via tests. In Figure 1 and 2, E, I, G and J represents the Young's Modulus, Moment of Inertia, Shear Modulus and Polar Moment of Inertia, respectively. The EI and GJ presented were normalized in order to protect confidential information.

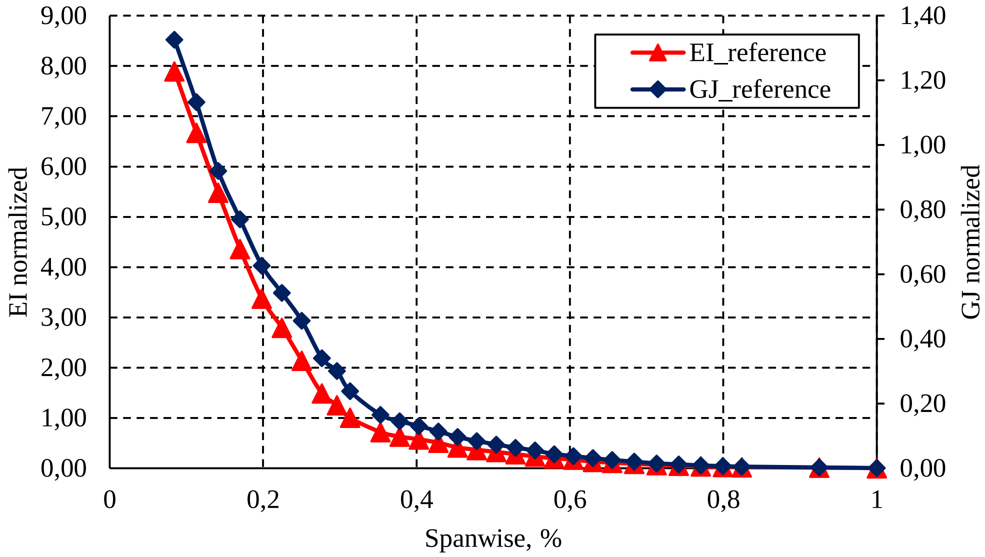

Figure 1: Reference Wing Stiffness - EI and GJ.

The stiffness curves, EI and GJ, obtained from the original ones were divided in two main groups of analysis. The first consists in shifted curves. This set of curves were obtained by multiplying the entire curve of EI and GJ by a determined factor. This factor represented a percentage of increase or decrease in wing rigidity, positive and negative percentage factors, respectively. Moreover, only one curve was varied at a time, EI or GJ. The percentage factor applied to the curves were from +10% to +50% and -10% to -50%. Therefore, a group of 20 different curves were determined, 10 varying only EI and keeping the original GJ and on the remaining curves keeping the original EI and varying only GJ. The second group consists in stiffness curves in which the rigidity of the wing was reproduced by Bezier parametric curves [6], as shown in Fig. 2, in order to vary the rigidity in a determined region of the wingspan.

Bezier curves are usually used in airfoils shape determination and optimization. The definition of a specific point in a Bezier curve follows the parametric function defined in Eq. (1).

DOI: 10.13009/EUCASS2017-480

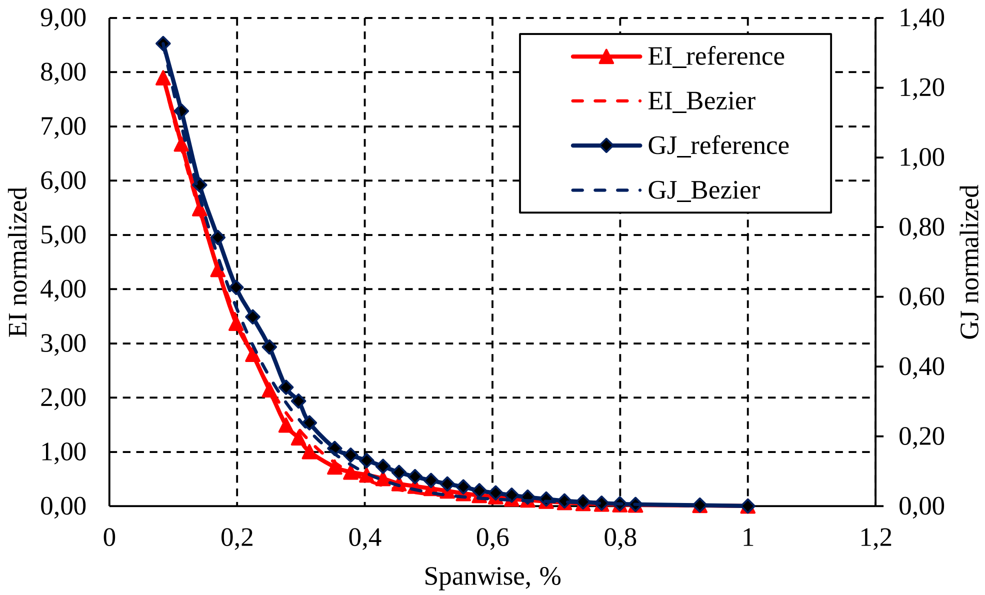

Figure 2: Original and Bezier parametric curves of EI and GJ.

$$P(t) = \sum_{i=0}^{k} P_i B_{i,k}(t) \qquad t \in [0,1] \qquad \textbf{(1)}$$

The $B_{i,k}(t)$ basis function are the k-th degree Bernstein polynomials [6]. The vector P_i represents the k+1 vertices of the control points. The intermediate control points attract the Bezier curve to themselves and influence the curve in their specific region.

A 7th degree Bezier curve was defined to determine the parametric curve, which means that eight control points could be varied in order to obtain new stiffness profiles. Therefore, the same variations applied to the shifted curves, as described before, were adopted to this group. Thus, for each control point, a set of 20 curves were obtained. Once the control points was spread along the wingspan, as shown on Table 2, it was possible to identify the influence of the variation on rigidity along the span wise. A total of 160 different stiffness curves compound this second group under analysis.

Table 2: Control Points and its relative coordinate on wingspan axle.

Control Point	**#1**	**#2**	**#3**	**#4**	**#5**	**#6**	**#7**	**#8**
Wingspan Relative Coordinate	0.0844	0.1984	0.2962	0.4284	0.5544	0.6552	0.7707	1

Four flight conditions were defined, considering a typical operation of the reference regional airplane, in order to perform the aerodynamic assessment. For all of them the Mach number was assumed the same, however, the Reynolds number (Re) and lift coefficient (C_L) was varied, according to Table 3. The intention here was to analyze the impact of the load distribution, different C_L, for a specific dynamic pressure (case conditions 1 and 2) and also assess the influence of dynamic pressure, different Qinf, on aerodynamic characteristics (case conditions 3 and 4).

Table 3: Case Condition Definitions.

Case Condition	**Mach**	**Re**	**C_L**	**Q_inf**
#1	0.82	1.81E+07	0.42	8.43E+03
#2	0.82	1.81E+07	0.577	8.43E+03
#3	0.82	3.02E+07	0.229	1.55E+04

DOI: 10.13009/EUCASS2017-480

#4	0.82	3.02E+07	0.314	1.55E+04

The numerical simulations were performed considering a full-potential solver with an integral boundary layer subroutine. The solver adopted to perform the required numerical simulations is the BLWF [7] solver. The BLWF has the capability to compute the parasite, induced and wave drag at a lower computational cost. Moreover, based on the simple beam theory, BLWF also computes the elastic effect (wing deflection and torsion) [8]. For its computational calculation, BLWF considers half of the body under analysis. Therefore, the main BLWF input parameters were define as per Table 4. For all calculations, the control parameter was the C_L, which means that the code realizes a set of calculations selecting the necessary angle of attack to guarantee the prescribed C_L value [8]. Moreover, all the simulations were performed considering a steady flight (1G).

Table 4: Main Input Arguments for BLWF.

Reference Wing Area [m2]	**Reference Chord [m]**	**Reference Span [m]**	**# Span Stations from the root to the wing tip**	**#Fuselage Stations**	**Fuselage Length [m]**	**Wing Chord @root [m]**	**Wing Chord @tip [m]**
46.28	3.6835	13.89	15	58	37.7	5.55	1.46

The analyses were conducted in 3 consecutive moments. The first aimed to assess the differences on the flow over the rigid and flexible reference wing for the reference stiffness curves. The next step, was the comparison of the reference flexible wing to the ones obtained with the stiffness shifted curves. The last but not the least, was the comparison of the reference flexible wing with all the 160 stiffness curves obtained with the Bezier parameterization. These steps are detailed on Table 5.

Table 5: Details of the main characteristics of each step of analysis.

STEP	**Aspect Ratio**	**Taper Ratio**	**Description**
#1	8.3	0.28	Reference wing - rigid vs flexible
#2	8.3	0.28	Reference Wing vs Shifted Curves
#3	8.3	0.28	Reference Wing vs Bezier Curves

3. Results

The impact of the wing flexibility in drag is assessed. Other parameters, such as wing loading, wing displacement and wing torsion are analysed if convenient for substantiating the results and their analysis. The results are presented from Section 3.1 and 3.2. First, the standard flexible wing is compared to a standard rigid wing. That is, both wings present the same geometry, however one is considered rigid while the other presents the reference value of flexibility. In the second part, the wing flexibility is analyzed through variations in the wing EI and GJ.

3.1 Rigid versus Flexible Wing

Fig. 3 shows the total drag and drag breakdown for the rigid and the flexible wings at the four different flight conditions presented in Table 3. The drag coefficient, presented in drag counts, is compared for the four different cases.

DOI: 10.13009/EUCASS2017-480

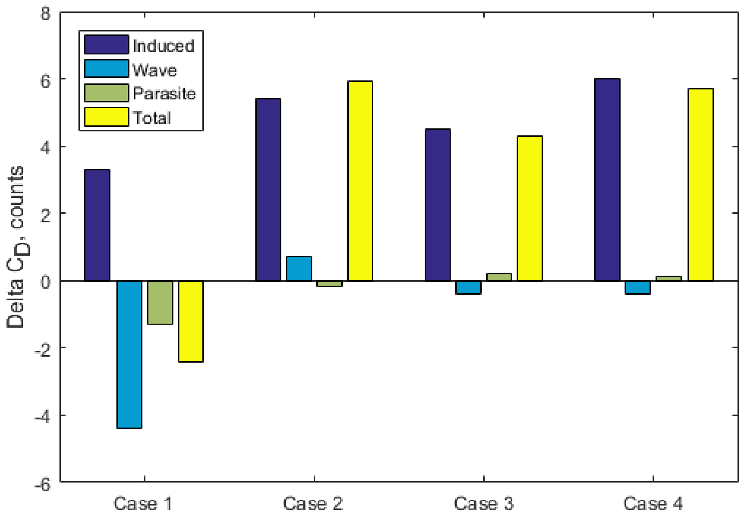

Figure 3. Drag breakdown comparison of rigid versus flexible wings for the four flight conditions.

This result shows that the total drag value is directly proportional to the C_L value of the flight condition. This is mainly due to a higher C_L incurring in a higher induced drag, but also in higher wave and parasite drags. Fig.4 indicates the comparison between the rigid and flexible wings for Case 01 and 02.

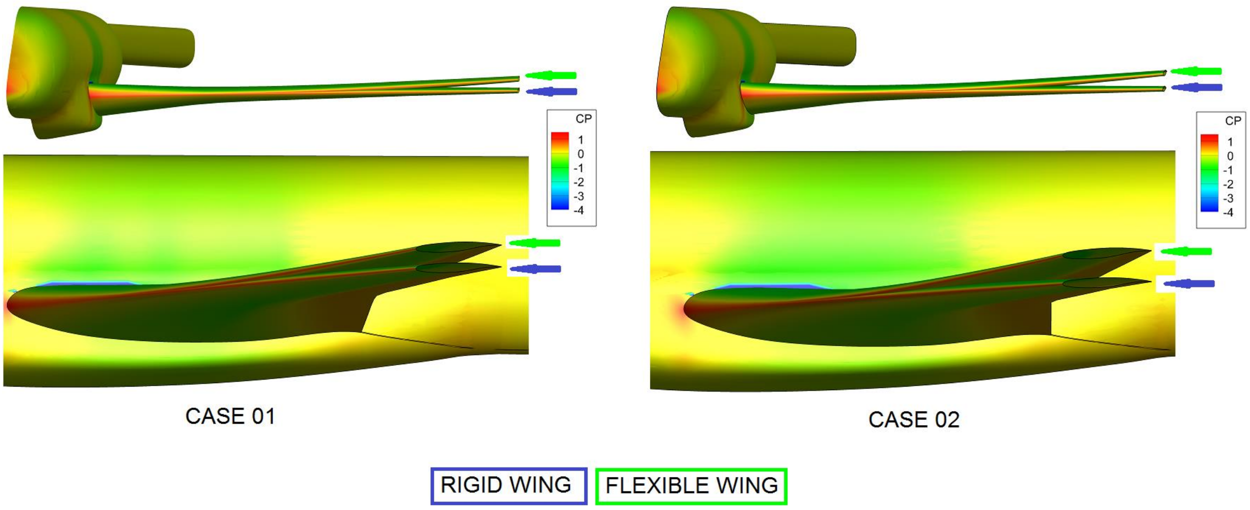

Figure 4. Drag breakdown comparison of rigid versus flexible wings for the four flight conditions.

In general, as indicated by cases 2, 3 and 4, the rigid wing presents a slightly lower total drag value than that of the flexible wing. The drag breakdown points out that this difference comes from the induced drag. The increase in induced drag for the flexible wing is due to the change in load distribution. For swept back wings, the wing tends to bend upwards during positive load factor maneuvers, which also causes a wash-out phenomenon due to the coupled torsion effect [5], that is, it presents negative torsion over the span. Thus, the wing tips are unloaded and the inner part of the wing is loaded, as presented in Fig. 5 [3]. This load distribution tends to distance itself from the optimal elliptical one, causing the increase in induced drag [9].

DOI: 10.13009/EUCASS2017-480

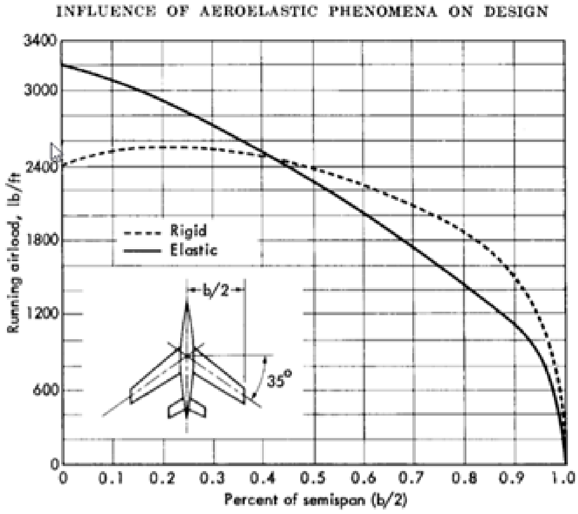

Figure 5. Airload distribution on swept rigid and elastic wing during a 2g maneuvering condition.[3]

The lift distributions over span comparison between the rigid and flexible wings for the four flight conditions is presented in Fig. 6, where the elliptical loading is shown in a dotted line for each of the conditions. The same behavior of Fig. 5 is observed: the flexible wing distances itself more from the elliptical loading than the rigid wing.

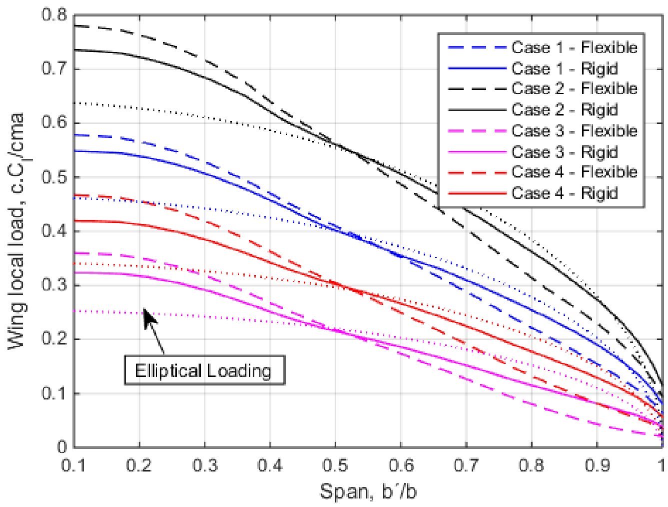

Figure 6. Wing loading over dimensionless span comparison of flexible, rigid and elliptical wings.

Since there is an unloading of the outer part of the wing, an increase in wing angle of attack is necessary in order to obtain a determined value of C_L. That is, flexible wings require a higher angle of attack in order to generate the same lift of a rigid wing. Table 6 summarizes the comparison on the angle of attack for a rigid and a flexible wing.

Table 6: Angle of attack [°] comparison between flexible and rigid wing.

Case	Flexible	Rigid
1	0.94	0.62
2	2.11	1.64
3	-0.35	-0.76

DOI: 10.13009/EUCASS2017-480

4	0.30	-0.22

Even though in most of the flight conditions the flexible wing presented a drag increase, in case number 1 an opposite effect was observed. The rigid wing presented a little over 2 drag counts more than the flexible wing. The trend for the induced drag is similar to the other cases, whereas the difference lies in the wave drag. A higher wave drag occurs in the rigid wing, as shown in Fig. 7. By comparing the streamlines of the upper surface of both wings, the rigid one presents a small flow separation, while the flow over the flexible wing remains attached.

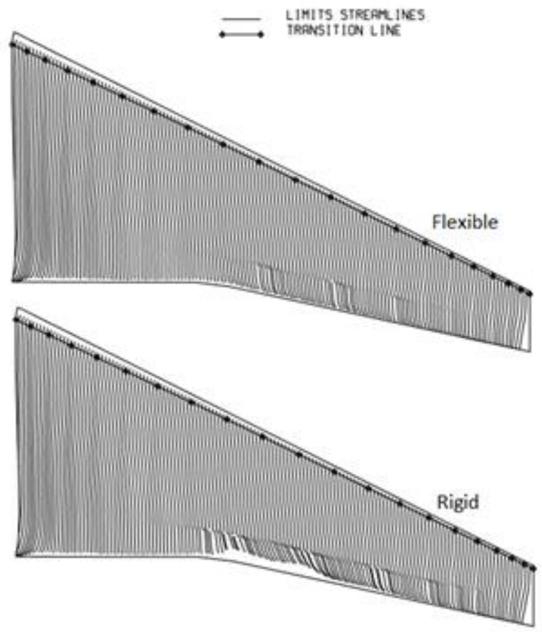

Figure 7. Upper surface streamlines for flexible and rigid wing.

The difference between the flow above the two wings comes from the torsion they are subjected to due to their respective flexibility. The rigid wing, by definition does not present any torsion due to the flow, while the flexible wing presents different values of torsion depending on the flight condition. Fig. 8 shows that for all the conditions, the wing presents a wash-out, as expected. In the region where the flow separation was observed, the flexible wing presents a smaller local angle of attack than the rigid wing, and this causes the flow to remain attached, incurring in less drag on the flexible than on the rigid wing.

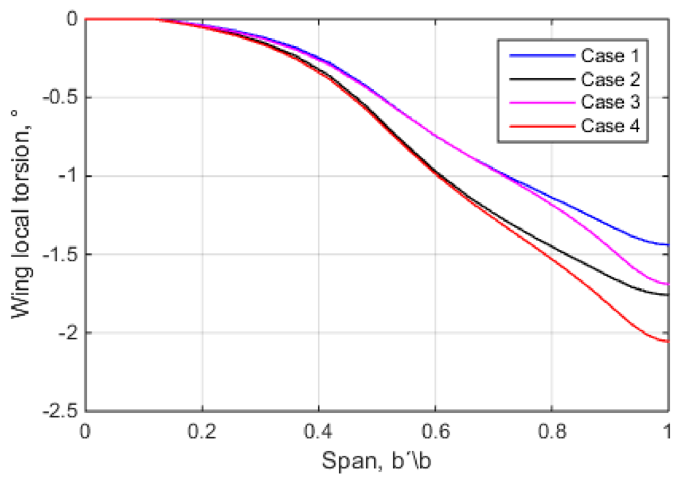

Figure 8. Torsion over dimensionless span for the flexible reference wing in the four flight conditions.

DOI: 10.13009/EUCASS2017-480

For the low C_L conditions (Cases 3 and 4), no separation was observed, while for the high C_L condition (Case 2), flow separation was observed for both the rigid and the flexible wing. Hence, no significant difference in wave drag is obtained for these cases.

3.2 EI and GJ Variations

The analysis of bending (EI) and torsional stiffness (GJ) variation due to the shifting of the curves for all Case conditions, as described on Section 2, are presented in the sub sections of Section 3.2.

3.2.1 Shifted Curves

The bending stiffness was compared for all cases and observed that, for the same Reynolds, higher C_L values causes greater impact in Drag, as shown in Fig. 9 and Fig. 10. This effect is related to the increase of Induced Drag, as shown in Fig. 11 and Fig. 12. Furthermore, Case 2 also had significant contribution of wave drag, indicating that this condition is above the aircraft design point.

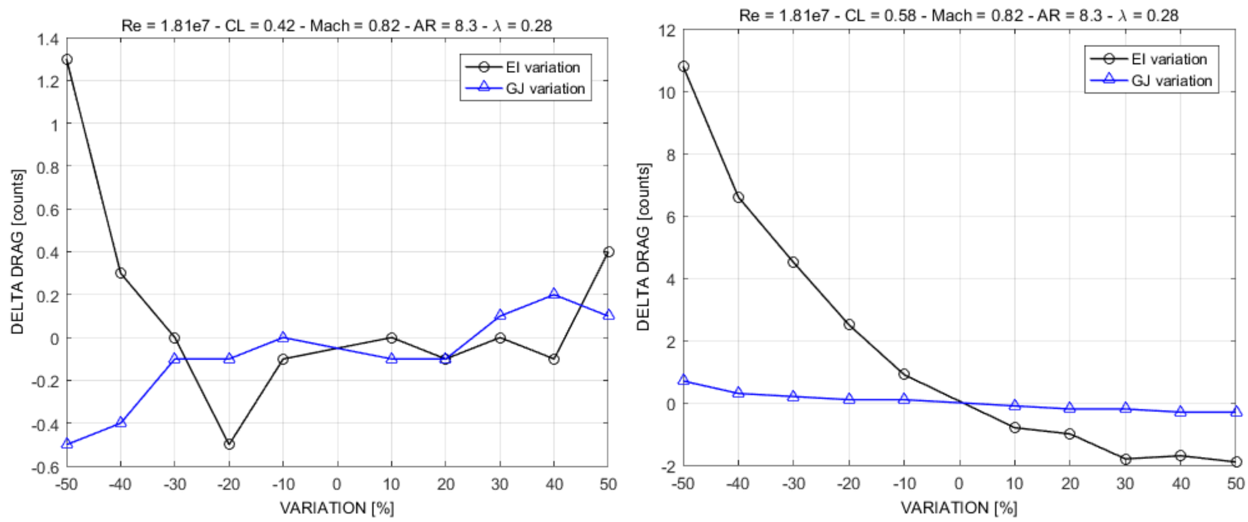

Figure 9. Delta Drag vs EI and GJ Variation, Case 1 (left) and Case 2 (right).

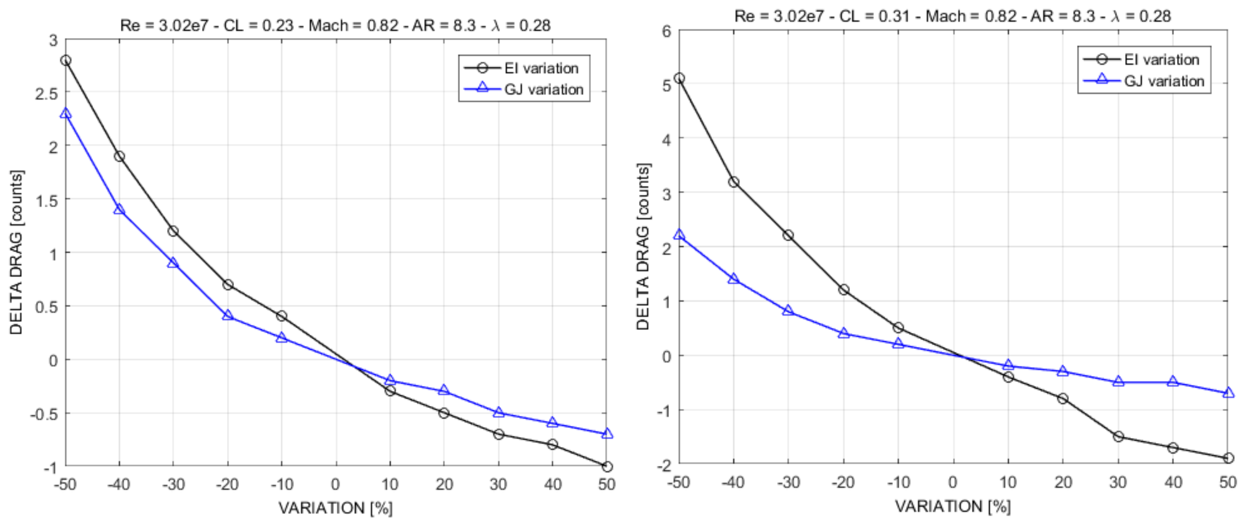

Figure 10. Delta Drag vs EI and GJ Variation, Case 3 (left) and Case 4 (right).

The behaviour of the Delta Drag Curve for Case 1, shown in Fig. 9, is different from the other cases when the stiffness is increased due to the detachment of the airflow over the upper surface, as shown in Fig. 13, caused by the formation of a stronger shock wave, which results in increase of the wave drag, as shown in Fig. 14.

DOI: 10.13009/EUCASS2017-480

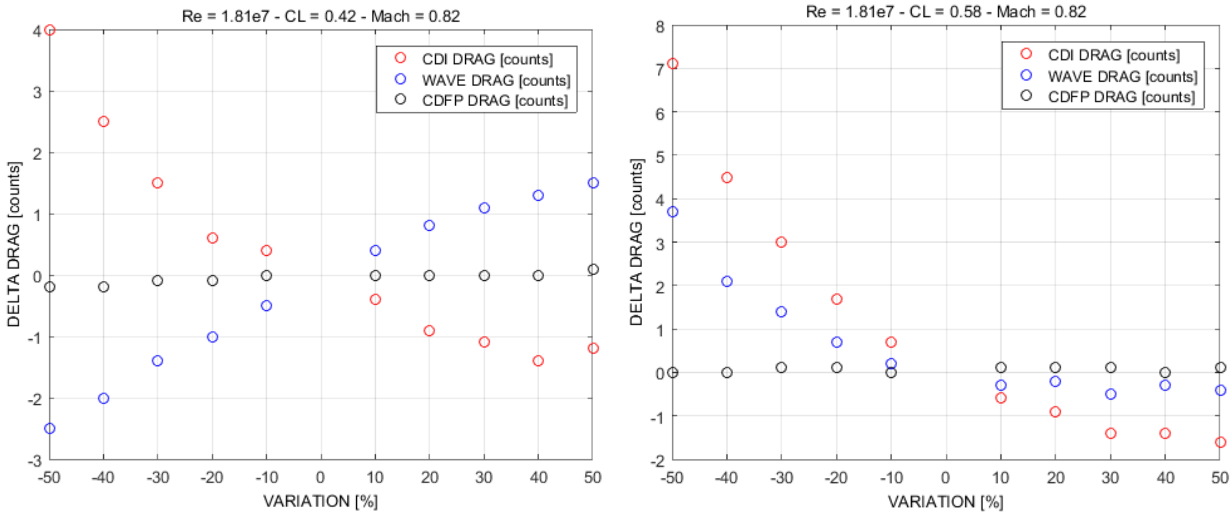

Figure 11. Delta Drag vs EI Variation, Case 1 (left) and Case 2 (right).

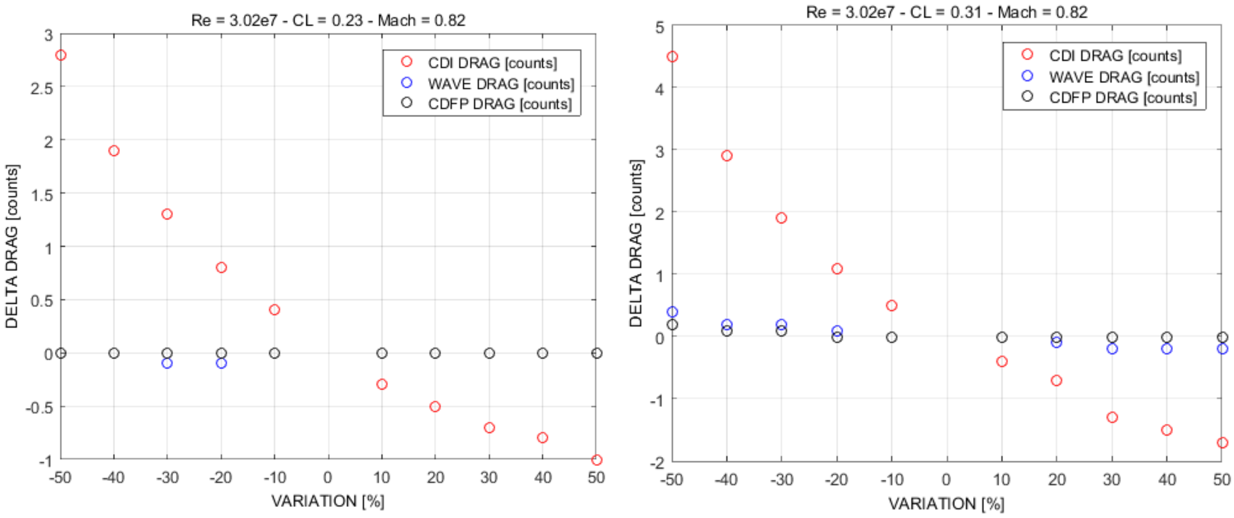

Figure 12. Delta Drag vs EI Variation, Case 3 (left) and Case 4 (right).

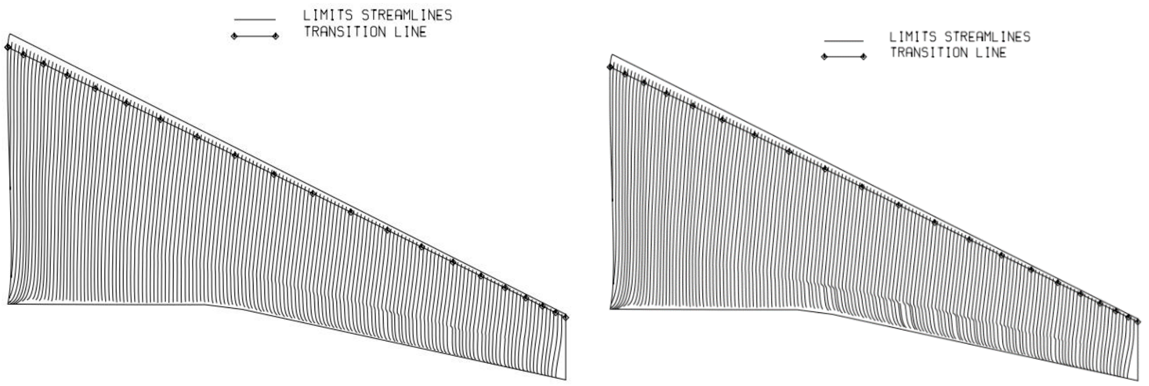

Figure 13. Upper surface streamlines, Case 1 -50% EI (left) and +50% EI (right).

DOI: 10.13009/EUCASS2017-480

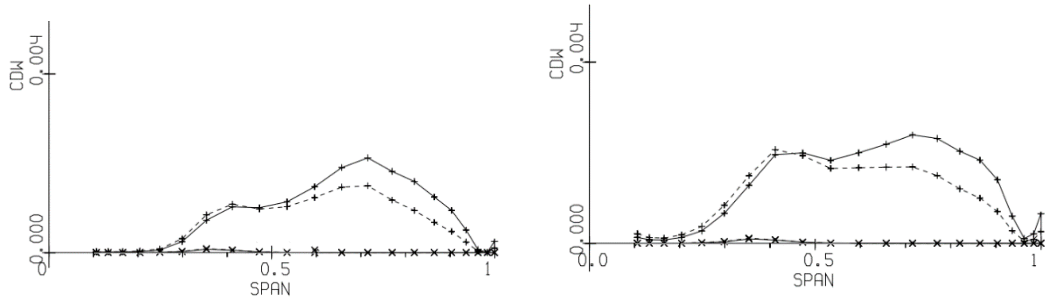

Figure 14. Wave Drag vs Span, Case 1 -50% EI (left) and +50% EI (right).

Based in Fig. 9 and Fig. 10, the effects of the dynamic pressures were compared for all running cases and verified that higher dynamic pressures had more influence on GJ variation due to the wing twist along the spanwise direction, represented in Fig. 15 and Fig. 16, as expected according to [10] and shown in Fig. 17.

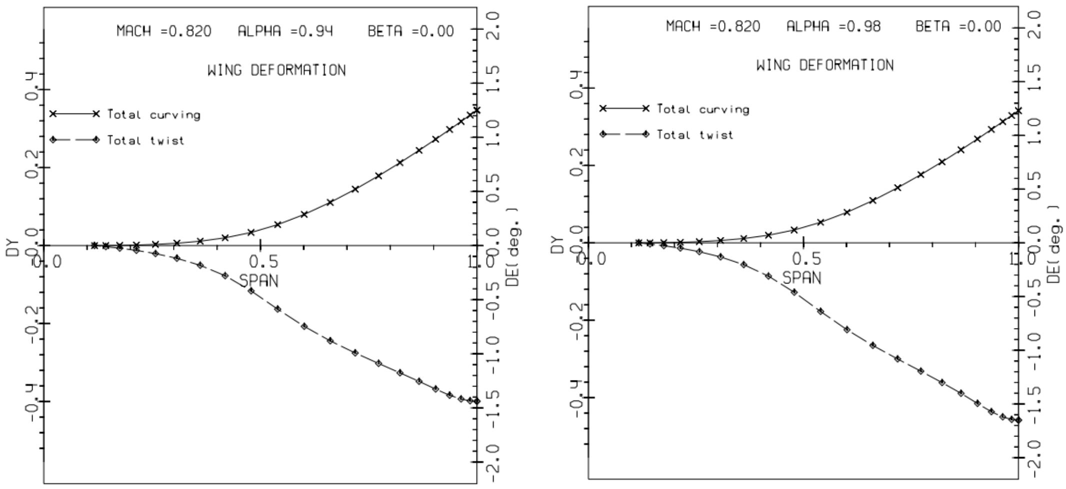

Figure 15. Bending and Twist vs Span, Case 1 reference (left) and -40% EI (right).

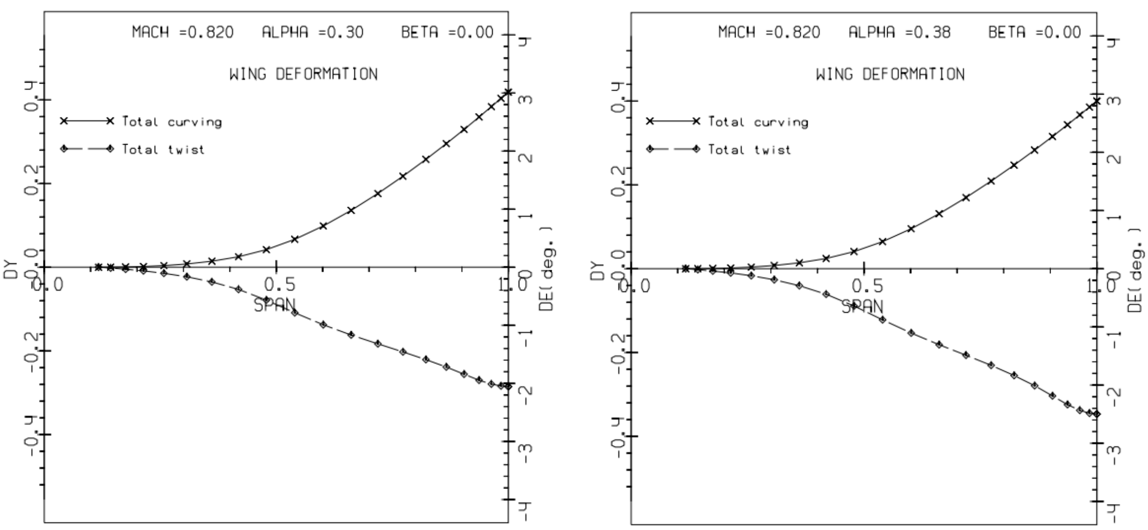

Figure 16. Bending and Twist vs Span, Case 4 reference (left) and -40% EI (right).

DOI: 10.13009/EUCASS2017-480

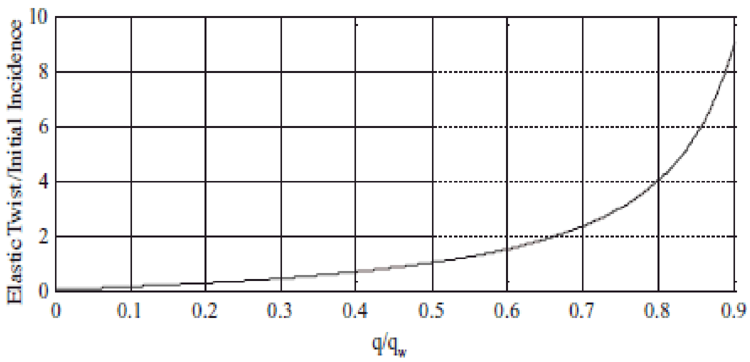

Figure 17. Typical twist behavior for two-dimensional airfoil with torsion spring from Ref. 5.

In the presence of higher twist values, the Lift distribution distances from the elliptical form, as shown in Fig. 18, which results in the increase of the induced drag, as shown in Fig. 19 and Fig. 20.

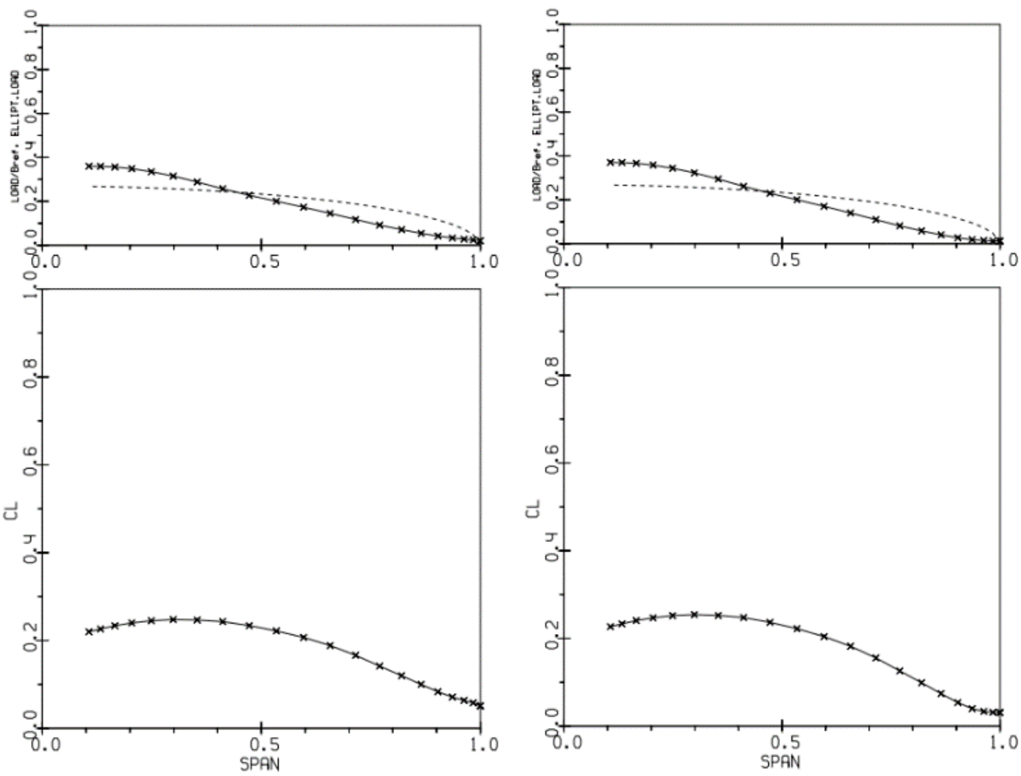

Figure 18. C_L and Lift vs Span, Case 3 reference (left) and -50% GJ (right).

DOI: 10.13009/EUCASS2017-480

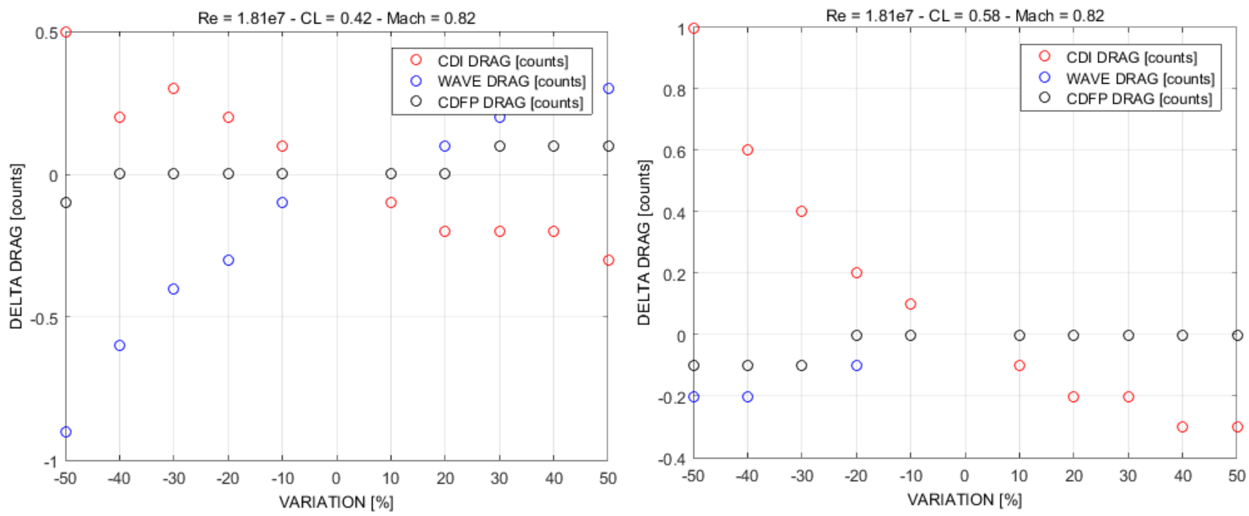

Figure 19. Delta Drag vs GJ Variation, Case 1 (left) and Case 2 (right).

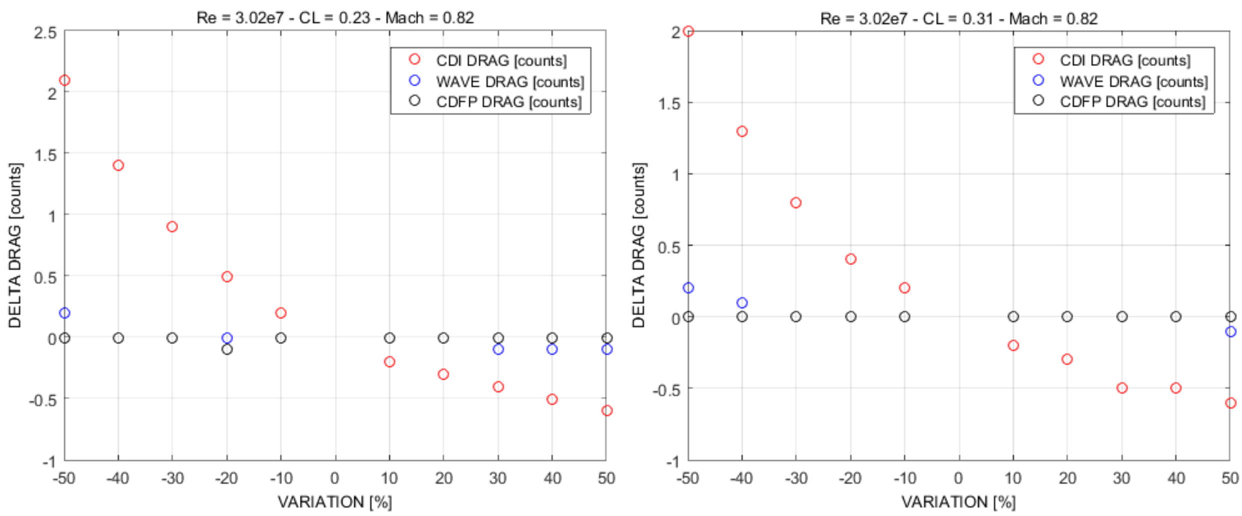

Figure 20. Delta Drag vs GJ Variation, Case 3 (left) and Case 4 (right).

The Wave Drag increase on Case 1, as shown in Fig. 19, due to GJ variation is resultant of a similar effect of flow detachment from the wing upper surface due to strong shock wave formation, which similar effect happened when EI was studied for this same Case, as shown in Fig. 13 and discussed previously.
The results of bending (EI) and torsional stiffness (GJ) variation due to control points profile, as described on Section 2, are presented in Section 3.2.2.

3.2.2 Control Points

For EI variation, the control points closer to the wing root have more influence on the resultant drag, as shown in Fig. 21 and Fig. 22, due to higher wing bending as result of stiffness reduction, as presented in Fig. 23.

DOI: 10.13009/EUCASS2017-480

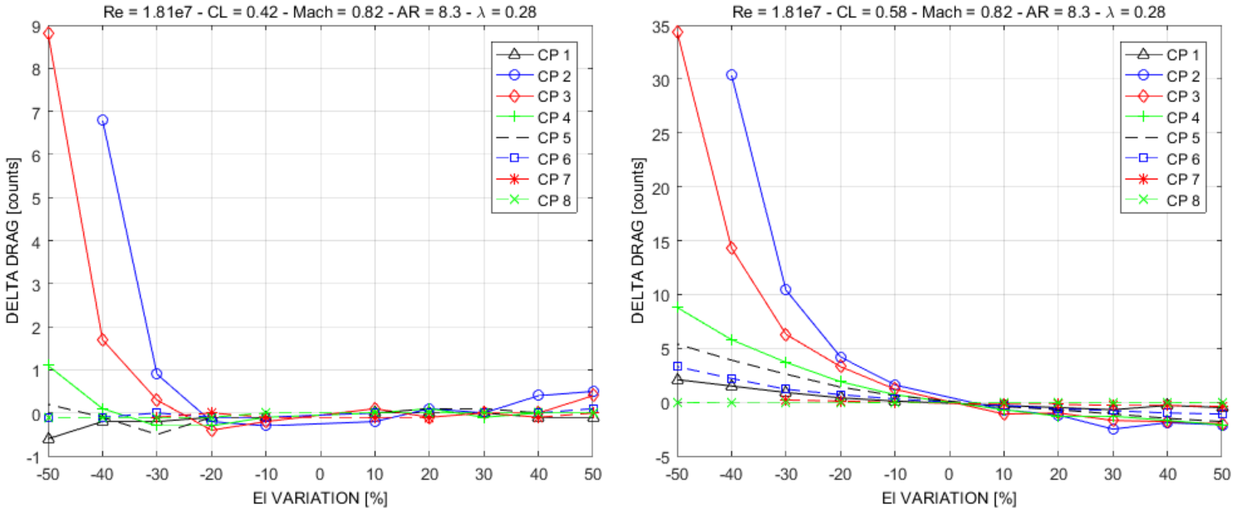

Figure 21. Delta Drag vs EI Variation, Case 1 (left) and Case 2 (right).

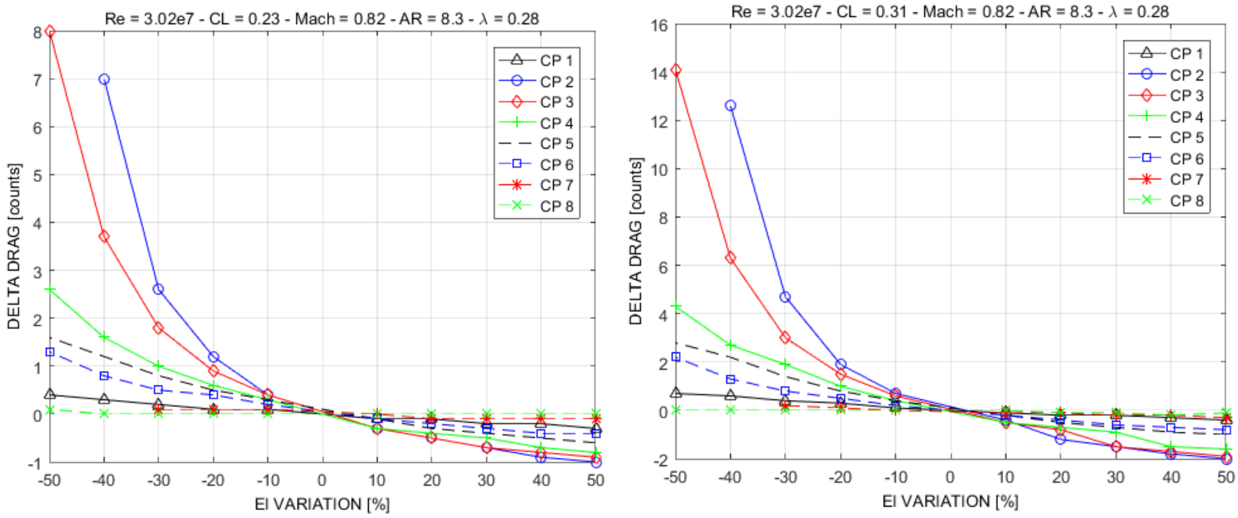

Figure 22. Delta Drag vs EI Variation, Case 3 (left) and Case 4 (right).

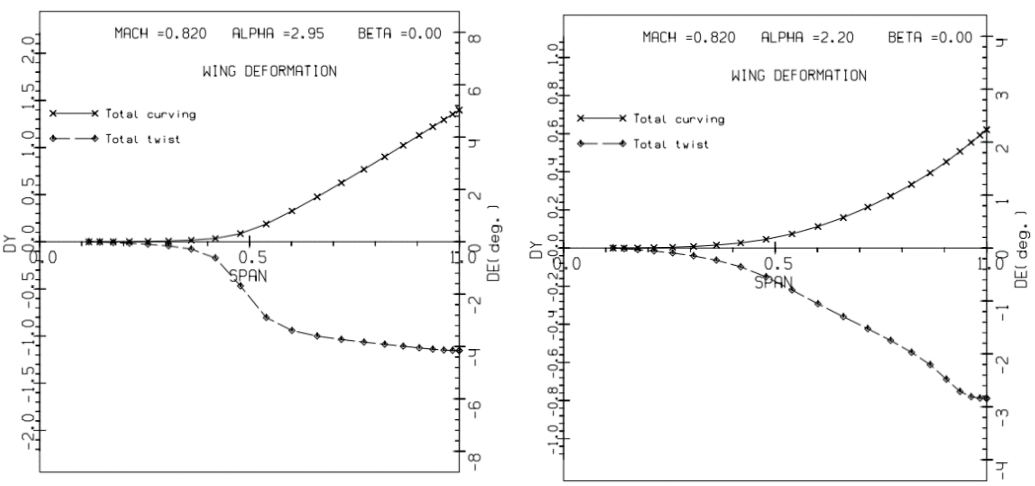

Figure 23. Bending and Twist vs Span, Case 2 CP3 -50% EI (left) and CP5 +50% EI (right).

DOI: 10.13009/EUCASS2017-480

The results presented in Fig. 24 and Fig. 25 for GJ variation in each control point is similar to the ones presented in Fig. 9 and Fig. 10 for the shifted curves.

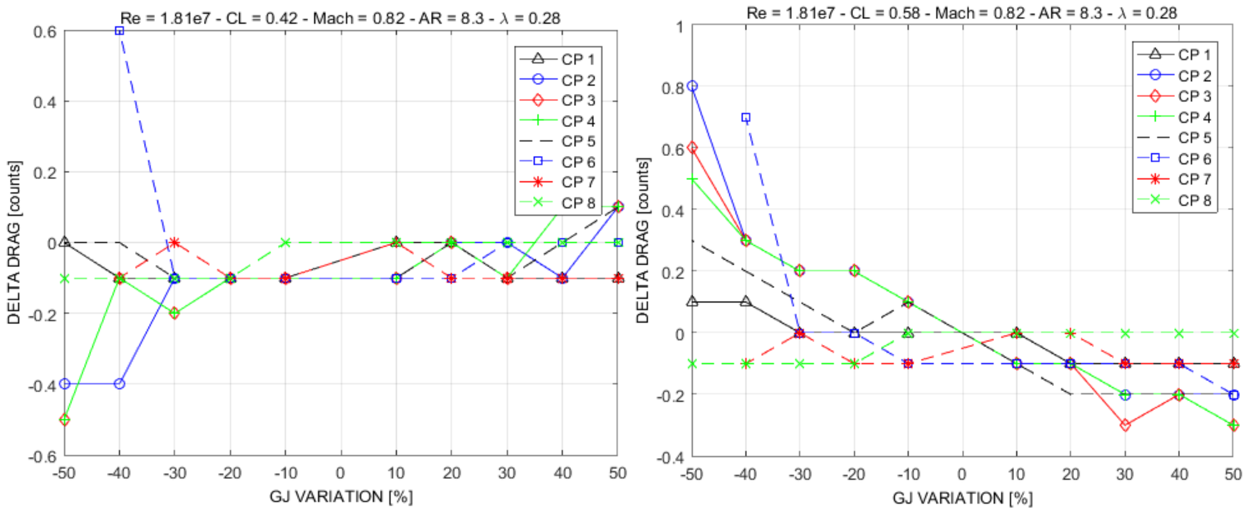

Figure 24. Delta Drag vs GJ variation, Case 1 (left) and Case 2 (right).

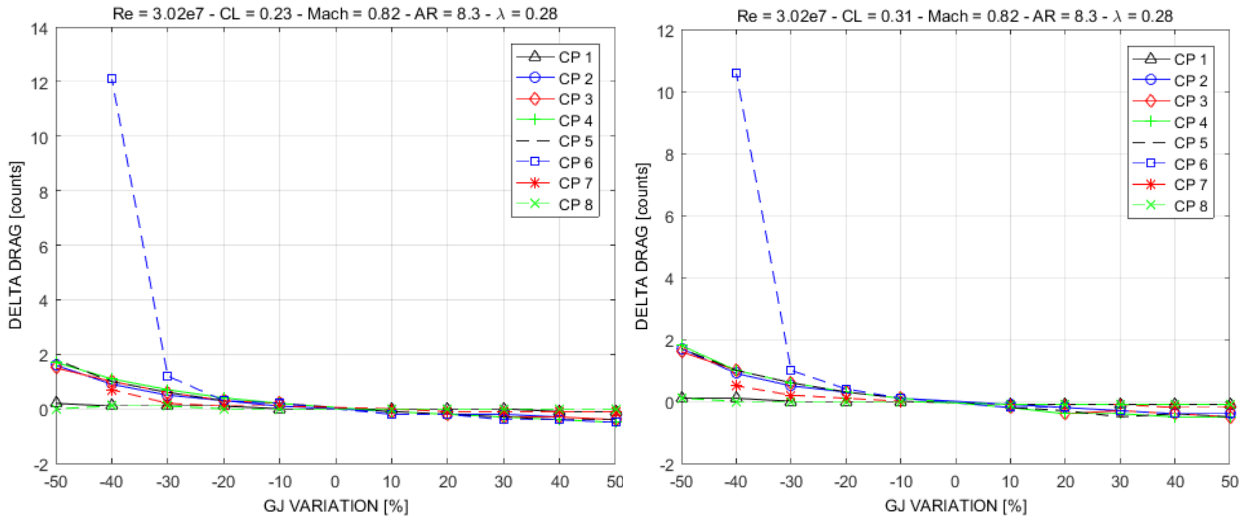

Figure 25. Delta Drag vs GJ variation, Case 3 (left) and Case 4 (right).

Some controls points are not presented in Fig. 21, Fig. 22, Fig. 24 and Fig. 25 due to convergence problems with BLWF, this effect is also represented on the sixth control point in Fig. 25, that shows a higher drag increase before the convergence problem on -50% GJ for this control point.

4. Conclusion

The effects of wing bending and torsional rigidity were analysed for a wing-body configuration of a regional aviation aircraft.
In general, the higher the dynamic pressure of the flight condition, the higher the drag variations. However, the highest drag variations in these analyses were observed for the flight condition with the highest C_L at lower dynamic pressure. Wing bending flexibility variations for shifted rigidity curves introduced an increase in up to 10 drag counts when compared to the standard flexible wing. For the torsional flexibility shifted variations, an increase of up to 3 drag counts was obtained.

DOI: 10.13009/EUCASS2017-480

For the rigidity curves obtained through variations on the control points, an increase of up to 35 drag counts was observed for the EI analysis, whereas for the GJ analysis no considerable changes in drag were observed. Changes in the control point closest to the wing-fuselage junction presented the highest impact on drag.
When compared flexible and rigid wings, the flexibility tends to increase the drag of the configuration. This is due to the bending and coupled torsion of the wing that tends to unload the wing tips and load the inner part of the wing in order to maintain the same C_L. The resulting aerodynamic load distribution distances itself from the optimal elliptical one, increasing induced drag. Furthermore, the wave drag plays a key role in the total C_D, as shown in Sections 3.2.1 and 3.2.3. Depending on the rigidity of the wing, its interaction with the flow might lead to some torsions and displacements that could impact the flow over the wing in such a manner that it could not be ignored during an early design phase.
Although, the tendencies in drag variation are similar for the flight conditions and flexibility and geometry variations, the flow separations due to shock waves is a main player on total drag. Therefore, a robust optimized design for cruise might evaluate, during the design phase, the flexible behaviour of the wing at the design point, i.e., determine the induced and wave drag after the accommodation of the wing to the flow over it.

References

[1] Smyth, M., and Pearce, B., “IATA Economics Briefing N°9: Air Travel Demand", International Air Transportation (IATA), April 2008.
[2] REGULATION (EU) No 598/2014 OF THE EUROPEAN PARLIAMENT AND OF THE COUNCIL of April 2014
[3] Bisplingohh, R.L., Ashley, H., Halfman, R.L., Introduction do Aeroelasticity, 2nd ed., Addison-Wesley, 1957, Chap. 1 and 2.
[4] Hodges, D.H., Pierce, G. A., Introduction to Structural Dynamics and Aeroelasticity, Cambridge University Press, Cambridge, 2002, Chap. 3.
[5] Weisshaar, T. A., Aircraft Aeroelastic Design and Analysis, School of Aeronautics and Astronautics – Purdue University, 1995, Chap. 1.
[6] Sohn, M. H., Lee, K. J, “Bezier Curve Application in the Shape Optimization of Transonic Airfoils”, AIAA-2000-4523, pp. 884-893
[7] Karas, O. V., and Kovalev, V. E., “BLWF 43 User’s Guide”, 2002
[8] Karas, O. V., and Kovalev, V. E., “BLWF 58 User’s Guide”, 2004
[9] Anderson, Jr., J. D., Fundamentals of Aerodynamics, 3rd ed., McGraw-Hill, New York, USA, 2001, Chap. 5.
[10] Wright, J., R., and Cooper, J., E., Introduction to Aircraft Aeroelasticity and Loads, 1st ed., John Wiley & Sons Ltd, England, 2007, Chap. 8.